Acta Crystallographica Section F
Structural Biology and Crystallization Communications
ISSN 1744-3091

High-resolution structure of an α-spectrin SH3-domain mutant with a redesigned hydrophobic core

Ana Cámara-Artigas,[a]* Monserrat Andújar-Sánchez,[a] Emilia Ortiz-Salmerón,[a] Celia Cuadri,[a] Eva S. Cobos[b] and Jose Manuel Martin-Garcia[a]

[a]Departamento de Química-Física, Bioquímica y Química Inorgánica, Universidad de Almería, Carretera Sacramento, Almería 04120, Spain, and [b]Departamento de Química-Física, Universidad de Granada, Avenida Fuentenueva s/n, Granada 18002, Spain

Correspondence e-mail: acamara@ual.es

Received 12 June 2010
Accepted 28 July 2010

PDB Reference: α-spectrin SH3-domain mutant, 3ngp.

The α-spectrin SH3 domain (Spc-SH3) is a small modular domain which has been broadly used as a model protein in folding studies and these studies have sometimes been supported by structural information obtained from the coordinates of Spc-SH3 mutants. The structure of B5/D48G, a multiple mutant designed to improve the hydrophobic core and as a consequence the protein stability, has been solved at 1 Å resolution. The crystals belonged to the orthorhombic space group $P2_12_12_1$, with unit-cell parameters $a = 24.79$, $b = 37.23$, $c = 62.95$ Å. This mutant also bears a D48G substitution in the distal loop and this mutation has also been reported to increase the stability of the protein by itself. The structure of the B5/D48G mutant shows a highly packed hydrophobic core and a more ordered distal loop compared with previous Spc-SH3 structures.

1. Introduction

The Src-homology 3 (SH3) domain is a small globular protein of about 60 residues which is formed by two orthogonal β-sheets, each of which is formed by three antiparallel β-strands. The loops connecting strands β1–β2, β3–β4 and β5–β6 are named the RT, n-Src and distal loops, respectively. Since the first structure of an SH3 domain, that of the wild-type chicken α-spectrin SH3 (Spc-SH3) domain, was solved by Musacchio and coworkers (Musacchio *et al.*, 1992), the structures of many different Spc-SH3 variants have been solved by means of X-ray diffaction (Musacchio *et al.*, 1992; Vega *et al.*, 2000; Berisio *et al.*, 2001; Casares, Lopez-Mayorga *et al.*, 2007) and NMR (Casares, Ab *et al.*, 2007).

The conformational equilibrium and the stability of the Spc-SH3 domain have been broadly characterized using spectrophotometric as well as calorimetric techniques (Viguera *et al.*, 1994). The folding of the Spc-SH3 domain at low ionic strength follows a two-state transition with no populated intermediates. This small domain is one of the best characterized proteins and has been the focus of model studies for the characterization of the folding pathways of proteins. Therefore, the Spc-SH3 domain has been chosen as a model system for studies of stability in proteins with a redesigned hydrophobic core (Ventura *et al.*, 2002). The hydrophobic core of the Spc-SH3 domain comprises nine residues: Val9, Ala11, Met25, Leu31, Leu33, Val44, Val53 and Val58. In order to design non-native novel sequences in the hydrophobic core of the SH3 domain the *Perla* algorithm was used and a series of 'artificial' sequences were obtained. These mutations were introduced into the α-spectrin SH3 nucleus to study the changes in stability. As a result, three groups of mutants, called C8A, Best4 and Best5, were subjected to kinetic and thermodynamic studies (Ventura *et al.*, 2002; Cobos *et al.*, 2003). In addition, to help in the analysis of the thermodynamic and kinetic data, the structures of some of these mutants were obtained (PDB codes 1e6g, 1e6h and 1h8k; Ventura *et al.*, 2002). All the new core mutants showed a similar thermal stability to the wild-type domain (Ventura *et al.*, 2002) and an increase in the kinetic constants of the corresponding folding and unfolding processes. The results suggested the stabilization of the transition state, probably owing to the strain induced by over-packing of the hydrophobic nucleus (Ventura *et al.*, 2002). In order to test this

hypothesis and to understand the origin of the thermodynamic behaviour of these mutants, the Best5 variant containing a Val residue instead of Ile25 (Best5-I25V, hereafter referred to as B5) was chosen and a set of additional mutations based on this variant were thoroughly studied by Cobos *et al.* (2003). However, only the structure of B5 was obtained (PDB code 1e7o). Unfortunately, this structure was solved using a low-quality data set, resulting in poor electron density in the difference maps used to model key protein residues.

A very interesting and common feature of all crystallographic structures of the Spc-SH3 domain is the presence of Asn47 in the distal loop in the forbidden region of the Ramachandran plot. The mutation of the aspartate at the adjacent position 48 to a glycine introduces a higher degree of freedom in the polypeptide chain in this loop. The structures of two mutants at position 48 have been solved in order to characterize this behaviour (Martinez *et al.*, 1998; Fernández-Escamilla *et al.*, 2004). In these structures, the turn adopts a more relaxed conformation and appears in the allowed region of the Ramachandran plot. On the other hand, a lack of electron density in the difference maps makes it difficult to model some residues in the β-turn and only limited information has been obtained from these structures.

With the goal of understanding the role played by the mutations of the hydrophobic core residues and additionally the mutation of aspartate 48 to glycine in the distal loop in the protein stability and folding kinetics, we have solved the structure of the B5/D48G mutant. Here, we describe the structure of the B5/D48G mutant at atomic (1 Å) resolution and compare our structure with those previously described for other redesigned core mutants and Asp48 mutants of the Spc-SH3 domain.

2. Materials and methods

2.1. Protein purification of the B5/D48G mutant

The B5/D48G mutant was obtained by the polymerase chain reaction (PCR) method. The fragment was cloned into the pBAT4 plasmid and expressed in *Escherichia coli* BL21 (DE3). Purification was achieved as described by Viguera *et al.* (1994). The sample was stored in 50 m*M* glycine–HCl pH 3.5 buffer and concentrated to 4 mg ml^{-1}. The protein concentration was determined by measuring the absorbance value at 280 nm and using an extinction coefficient of 16 150 cm^{-1} M^{-1} as obtained by the method of Gill & von Hippel (1989). The sequences of the α-spectrin SH3-domain and B5/D48G proteins are compared in Fig. 1. In this figure the sequences of all the hydrophobic core mutants of the Spc-SH3 domain of known structure are also shown.

Table 1
Data-collection and refinement statistics.

Values in parentheses are for the highest resolution bin.

Space group	$P2_12_12_1$
Unit-cell parameters (Å)	a = 24.79, b = 37.23, c = 62.95
Resolution range (Å)	20–1.08
No. of observations	87782 (11438)
Unique reflections	25256 (3590)
Data completeness (%)	99.2 (98.4)
$R_{\rm merge}$† (%)	7.1 (33.2)
$\langle I/\sigma(I)\rangle$	11.1 (3.2)
Average multiplicity	3.5
Wilson B factor (Å^2)	9.37
Refinement	
Protein residues	56
Solvent molecules	66
$R_{\rm work}$ (%)	16.8
$R_{\rm free}$ (%)	18.5
R.m.s. deviations from ideal geometry	
Bonds (Å)	0.005
Angles (°)	1.005
Mean B (protein) (Å^2)	12.3
Mean B (nonprotein) (Å^2)	32.04
Residues in allowed regions of the Ramachandran plot‡ (%)	100

† $R_{\rm merge} = \sum_{hkl}\sum_i |I_i(hkl) - \langle I(hkl)\rangle| / \sum_{hkl}\sum_i I_i(hkl)$, where $I_i(hkl)$ is the ith observation of reflection hkl and $\langle I(hkl)\rangle$ is the weighted average intensity for all observations i of reflection hkl. ‡ From *PROCHECK* statistics.

2.2. Crystallization and data collection

Crystals of the B5/D48G mutant of the Spc-SH3 domain were obtained by mixing 4 µl protein solution at 4 mg ml^{-1} with 2 µl precipitant solution composed of 2 *M* ammonium sulfate and 0.1 *M* MES pH 6.5. The protein drop was allowed to equilibrate against 1 ml precipitant solution at 298 K and crystals appeared in one week. For data collection, the crystals were soaked in a cryoprotectant solution containing 10% glycerol, looped and flash-frozen in liquid nitrogen. X-ray diffraction data collection was performed on beamline ID23-1 of the European Synchrotron Radiation Facility (ESRF) using a wavelength of 0.976 Å and an ADSC Quantum Q315r detector. To compensate for saturation of the detector by intense low-resolution reflections, two data sets, corresponding to high- and low-resolution reflections, were collected at two crystal-to-detector distances. Data were indexed and integrated using *iMOSFLM* (Leslie, 2006; Powell *et al.*, 2007). Scaling and merging were performed with the *CCP*4 program *SCALA* (Evans, 2006). The resulting crystallographic parameters and statistics of data collection are listed in Table 1.

2.3. Structure solution and refinement

The structure of the B5/D48G mutant was solved using the *PHENIX* software package (Zwart *et al.*, 2008). Firstly, the quality of

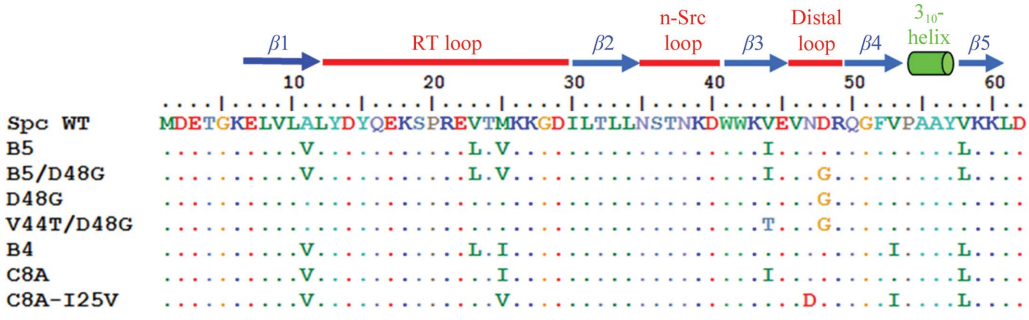

Figure 1
Sequence alignment of the hydrophobic core and distal loop mutants of known structure with respect to the wild-type protein. The residues are colour-coded according to the character of the amino acids. Residues conserved with respect to the wild type are represented as dots.

the data was checked using the program *phenix.triage*. The data showed a completeness of 91% in the inner resolution shell and 98.4% in the outer shell. The mutant crystals belonged to the orthorhombic space group $P2_12_12_1$ and the asymmetric unit consists of just one polypeptide chain, with a Matthews coefficient of 2.08 Å^3 Da^{-1} (40.96% solvent content). The initial structure of the B5/D48G mutant was determined by molecular replacement with the *AutoMR* wizard. The coordinates of wild-type Spc-SH3 (PDB entry 1shg; Musacchio *et al.*, 1992) were used as the search model. After molecular replacement with *Phaser*, the mutated residues were automatically built into the model using the *AutoBuild* wizard and manual building between cycles of refinement using *phenix.refine* was performed using the graphics program *Coot* (Emsley & Cowtan, 2004) using σ_A-weighted ($2F_o - F_c$) and ($F_o - F_c$) electron-density maps. In the early stages of refinement, simulated-annealing cycles of refinement were combined with minimization cycles and individual restrained isotropic ADP (atomic displacement parameters) refinement. Water molecules were automatically upgraded after each refinement cycle and manual inspection was performed using *Coot*.

Once the model was complete and the *R* factors had reached a minimum value (*R* of 18.7% and R_{free} of 20.2%), the weights between X-ray target and stereochemistry or ADP restraints were optimized in each macrocycle of the refinement and individual restrained anisotropic ADP refinement was performed. The anisotropic refinement was not applied to the parts of the model with high *B* factors, residues in alternative conformations and solvent molecules.

The quality of the model was also assessed using *MolProbity* (Chen *et al.*, 2010), which was used as an active validation tool as soon as a model was available for each rebuilding/refinement loop in *phenix.refine*. The atomic coordinates of the mutant have been deposited in the the PDB with accession code 3ngp.

Several programs from the *CCP*4 suite were used to analyse and compare the structure of the B5/D48G mutant (Collaborative Computational Project, Number 4, 1994): superposition and calculation of r.m.s. deviations of the structures were accomplished using *LSQKAB* (Kabsch, 1976), accessible surface areas were calculated using *AREAIMOL*, distances between amino acids were calculated using the program *CONTACT* and *B*-factor plots were generated using the program *BAVERAGE*. Finally, protein interfaces in the crystals were characterized using the *PISA* web server (Krissinel & Henrick, 2005). The final refinement statistics are presented in Table 1.

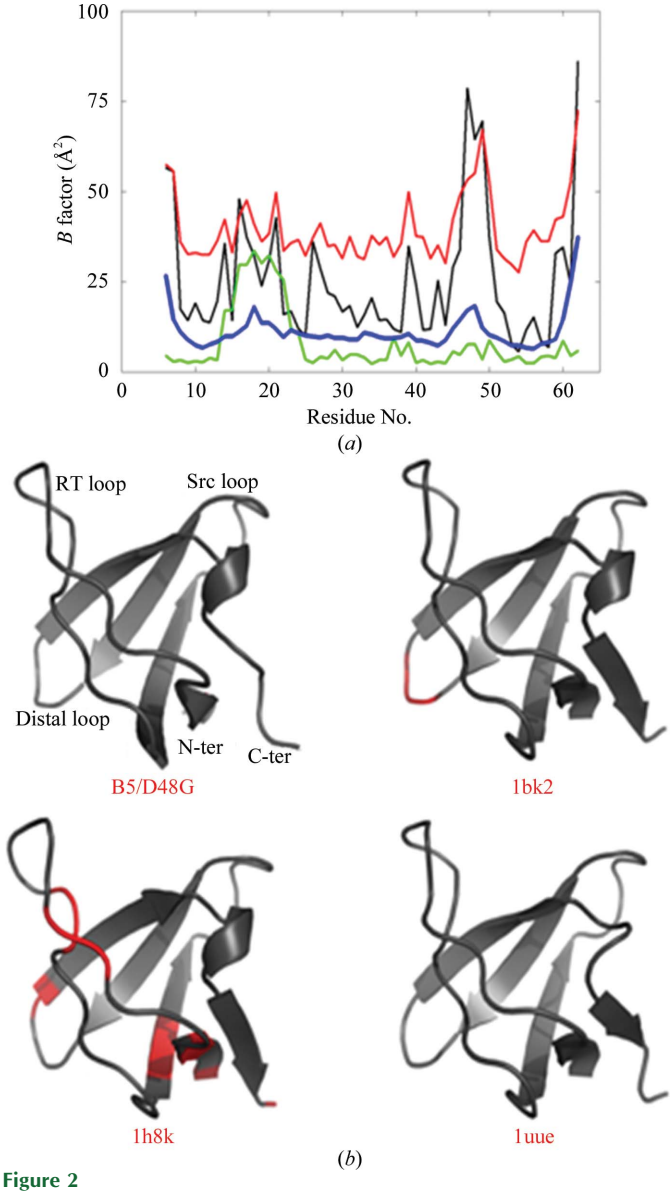

Figure 2
(*a*) *B*-factor plot of the B5/D48G mutant (PDB code 3ngp; blue), D48G mutant (1bk2; red), C8A-I25V mutant (1h8k; green) and V44T/D48G mutant (1uue; black). (*b*) Overall fold of the structures of the residues in the distal loop. Residues with occupancies of lower than 1 are shown in red.

3. Results and discussion

3.1. B5/D48G mutant crystallization

Crystals of the B5/D48G mutant were obtained under the same conditions used to crystallize other Spc-SH3 mutants and the wild-type protein. Only a few rectangular prism-shaped crystals appeared after one week of equilibration of the drop against the precipitant solution in a vapour-diffusion setup. This behaviour is quite different from that found for the crystallization of the wild-type protein, which was characterized by the very rapid growth of crystals in the presence of ammonium sulfate or sodium formate as the precipitant agent. An analysis of the protein interfaces present in the crystal structure of the wild-type protein showed that the second interface contains a major contact formed by Pro20 in the RT loop, which is packed against the aromatic residues Tyr13–Tyr57 of the symmetry-related molecule with a geometry similar to that found in the binding site of the SH3 domain with polyproline-rich sequences. Therefore, the rapid growth of these crystals has been attributed to this pseudo-binding effect, which accelerates the rate of crystal growth (Cámara-Artigas *et al.*, 2009). Interestingly, although the crystal of the B5/D48G mutant also belongs to the orthorhombic space group $P2_12_12_1$ the differences in the unit-cell parameters result in a different packing and the protein interfaces calculated using the *PISA* web server (Krissinel & Henrick, 2007) do not contain Pro20 in any of the crystal contacts. This may explain the slow growth of the crystals compared with other Spc-SH3 crystals.

3.2. B5/D48G mutant overall structure

The overall three-dimensional structure of the B5/D48G mutant is the same as those reported for the wild-type protein and other Spc-SH3 variants: a single β-barrel hydrophobic core formed by two perpendicular three-stranded β-sheets. Despite the high quality of the data collected, only 56 resides were modelled out of a total of 62. As previously described, the amino-terminal region of the Spc-SH3 domain is very flexible and has not been modelled in most Spc-SH3 structures (Cámara-Artigas *et al.*, 2009). As a consequence, about

10% of the protein is unmodelled and this results in higher R and R_{free} factors than expected for a high-resolution structure.

All of the residues of the structure of the B5/D48G mutant are placed in favoured regions of the Ramachandran plot. However, most structures of the Spc-SH3 domain have residue Asn47 outside the most favoured regions of the Ramachandran plot. This residue is located at the tip of the distal β-turn, which is formed by residues Val46-Asn47-Asp48-Arg49 and exhibits a slightly different conformation in each of the crystal structures deposited in the PDB, as can be observed in Fig. 2. This variability in the distal β-turn conformation has been related to an intrinsic low stability of the loop (Martínez & Serrano, 1999; Morel *et al.*, 2006).

3.3. Comparison with the structures of previous D48G mutant structures

Thermodynamic and kinetic studies of the Spc-SH3 domain point towards the residues of the distal loop playing a relevant role in the protein-folding process. Thus, in order to study the role of this loop in such a process, the structures of the D48G and N47D mutants have been solved (Martinez *et al.*, 1998; Ventura *et al.*, 2002; Fernández-Escamilla *et al.*, 2004). However, the *B*-factor plots of these structures showed higher than average *B* factors for the residues in this loop (Fig. 2*a*). Together with the low occupancy found for the loop residues in most of the available structures (Fig. 2*b*), this indicates poor electron density in the difference maps, which makes it difficult to model the loop. This is a common feature of almost all of the structures solved for Spc-SH3; the variability in the positions of the residues in this loop found among them is likely to be attributable to a lack of the electron density required to properly model these residues. In fact, the presence of multiple conformations in the available structures of the mutants at the distal loop, together with the *B*-factor plots, indicates high flexibility in this loop. In the structure of the B5/D48G mutant the *B* factors of the residues in the distal loop are only slightly higher than the average and the occupancies of all the residues in the loop are 1. The mutation of an aspartate residue to glycine introduces more degrees of freedom into the loop; at the same time, the turn can adopt a more relaxed conformation. However, as indicated by the *B*-factor and occupancy data, the loop is better defined in the electron density of the difference maps and this allows us to determine that this loop shows a type I′ conformation (Fig. 3). This is in agreement with the prediction that Asn-Gly at positions $i + 1$ and $i + 2$ is an optimal sequence for a two-residue β-turn in a β-hairpin which reduces the barrier to the folding process (Martinez *et al.*, 1998).

Analysis of the protein interfaces using the *PISA* web server indicates that the residues in the distal loop of the B5/D48G mutant participate in crystal contacts. For these residues, the accessible surface area (ASA) buried upon formation of the interface in the crystal is 230 Å^2, while in the wild-type structure the ASA buried by the same residues is only 73 Å^2. In both structures the residues in the distal loop are implied in hydrogen-bond interactions. However, in the B5/D48G mutant structure the higher ASA buried in the crystal interface, together with the optimal sequence of the β-turn, is expected to contribute to the better definition of this loop in the electron density in the difference maps.

3.4. Comparison with the structures of hydrophobic core mutants

More than 30 different mutants of the hydrophobic core of Spc-SH3 have been characterized by thermodynamic and kinetic techniques (Ventura *et al.*, 2002; Cobos *et al.*, 2003; Fernández-Escamilla *et al.*, 2004). However, the structures of only four of these mutants have been solved at high resolution. For the first time, the structure of a mutant of the hydrophobic core of the SH3 domain has been solved at a resolution near 1 Å.

The most similar structure is that of the B5 mutant (PDB code 1e7o; Cobos *et al.*, 2003), which includes the following mutations in the hydrophobic nucleus related to the Spc-SH3 domain: A11V, V23L, M25V, V44I and V58L. All of these residues are buried in the wild-type structure, with an overall accessible surface area (ASA) of lower than 10 Å^2. The mutations in the B5/D48G mutant affect the same five residues of the hydrophobic core (Fig. 1). As expected, these residues are also buried in the hydrophobic core of the structure of the B5/D48G mutant. However, when we compare the structure of this mutant with that of the B5 mutant, several important differences arise. From the B5 mutant structure solved at 3 Å resolution, it has been proposed that the positions of the side chains of the residues Val9, Leu31 and Leu33 are in the same conformation as in the wild-type structure. However, in the B5/D48G mutant a noticeable displacement of these side chains is found when compared with the B5 mutant and these displacements are also found in the backbone chain. As can be seen from the r.m.s.d. plot, these differences are also present when the B5/D48G mutant and wild-type structures are compared (Fig. 4).

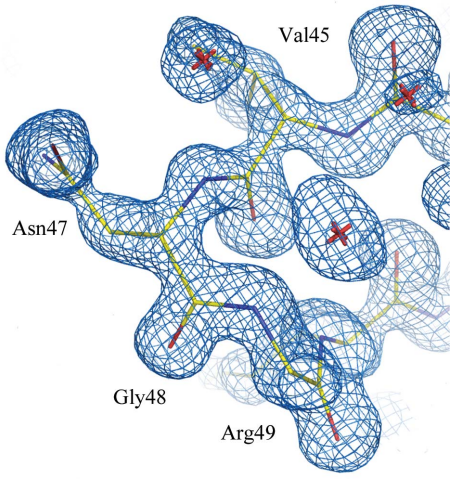

Figure 3
Distal loop $2F_o - F_c$ map contoured at 1σ.

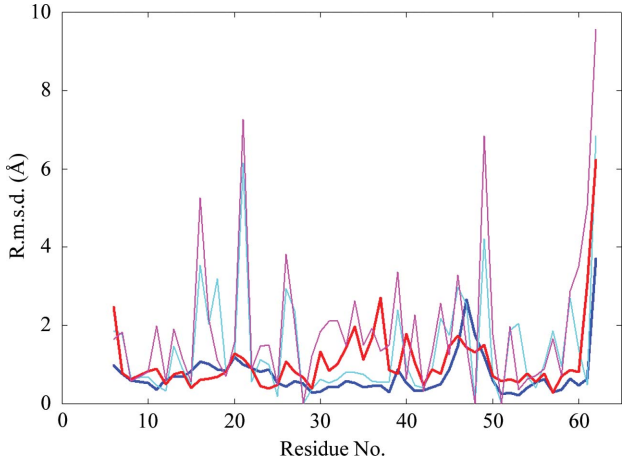

Figure 4
R.m.s.d. of the superposition of the coordinates of the B5/D48G mutant on those of the B5 mutant (red, main chain; pink, side chain) and the wild type (blue, main chain; cyan, side chain).

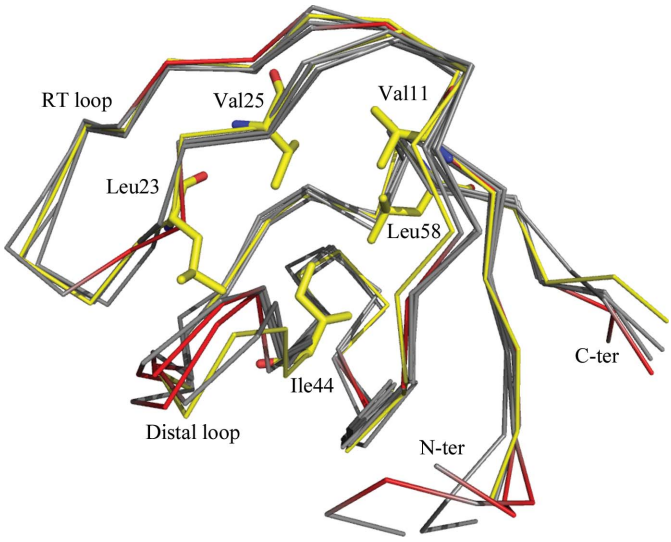

Figure 5
Main-chain superposition of the coordinates of the hydrophobic core (B5 mutant, PDB code 1e7o; Best4 mutant, 1e6h; C8A mutant 1e6g; C8A-125V mutant, 1h8k) and distal loop mutants. The backbones are shown in grey and residues with low occupancy are shown in red. The backbone of the B5/D48G mutant is shown in yellow and the mutated residues are shown in stick representation.

Comparison of the B5/D48G mutant with other hydrophobic core mutants shows the same differences in the backbone and side-chain positions as are found in the B5 and wild-type structures. The major differences are found in the RT and distal loops (Fig. 5). This variability in the loop conformations can be produced by the loss of a salt bridge between Glu16 and Arg49 of the RT and distal loop, respectively. In fact, this salt bridge is lost in all of the available structures of the hydrophobic core mutants and is only present in the Best4 mutant (PDB code 1e6h; Ventura *et al.*, 2002). In this mutant Met25 is replaced by an isoleucine and this substitution does not produce a displacement in the backbone of the nearby residues, as the volumes occupied by the two residues are almost identical. However, the replacement of the original valine at position 23 by the bulkier residue leucine in the B5/D48G mutant produces a displacement of the backbone, which simultaneously increases the distance between the backbone atoms of the residues in the RT and distal loops.

Kinetic and thermodynamic measurements performed on the B5 mutants demonstrated that the B5/D48G mutant was the most stable. The ΔG_{FU} values obtained were 12.4, 17.2, 19.2 and 24.2 kJ mol^{-1} for the wild type and the D48G, B5 and B5/D48G mutants, respectively, at pH 3.5 and 298 K (Cobos *et al.*, 2003). The more relaxed conformation of the distal loop as a consequence of the D48G mutation increases the stability of the Spc-SH3 domain. Additionally, the burial of the hydrophobic residues is the major driving force for the folding and the improved hydrophobic core packing accelerates the folding and increases the stability of the protein. The B5/D48G mutant takes advantage of both stabilizing effects and is the most stable of the mutants of the B5 variant.

4. Conclusions

This is the first time that an atomic resolution structure of a hydrophobic core mutant of the Spc-SH3 domain has been obtained. The improved quality of the structure will allow us to analyze the thermodynamic and kinetic aspects of the folding of the redesigned hydrophobic core mutants of the Spc-SH3 domain in more detail. This structure is well suited to test the importance of the role of the β-turn in the distal loop of the Spc-SH3 domain to modulate the protein stability and the folding kinetics. Additionally, the high-resolution structure reported in this work provides helpful information for use in future studies of hydrophobic core mutants of other proteins.

This research was funded by grants BIO2009-13261-C02-01 and BIO2009-13261-C02-02 from the Spanish Ministry of Education and Sciences and grants BIO-014 and P09-CVI-5063 from the Andalusian Regional Government. We would also like to thank Professor J. A. Gavira and the Project 'Factoría Española de Cristalización' for data collection and Professor Jose-Carlos Redondo-Olmedilla for revising the English text.

References

Berisio, R., Viguera, A., Serrano, L. & Wilmanns, M. (2001). *Acta Cryst.* D**57**, 337–340.
Cámara-Artigas, A., Andújar-Sánchez, M., Ortiz-Salmerón, E., Cuadri, C. & Casares, S. (2009). *Acta Cryst.* D**65**, 1247–1252.
Casares, S., Ab, E., Eshuis, H., Lopez-Mayorga, O., van Nuland, N. A. & Conejero-Lara, F. (2007). *BMC Struct. Biol.* **7**, 22.
Casares, S., López-Mayorga, O., Vega, M. C., Cámara-Artigas, A. & Conejero-Lara, F. (2007). *Proteins*, **67**, 531–547.
Chen, V. B., Arendall, W. B., Headd, J. J., Keedy, D. A., Immormino, R. M., Kapral, G. J., Murray, L. W., Richardson, J. S. & Richardson, D. C. (2010). *Acta Cryst.* D**66**, 12–21.
Cobos, E. S., Filimonov, V. V., Vega, M. C., Mateo, P. L., Serrano, L. & Martínez, J. C. (2003). *J. Mol. Biol.* **328**, 221–233.
Collaborative Computational Project, Number 4 (1994). *Acta Cryst.* D**50**, 760–763.
Emsley, P. & Cowtan, K. (2004). *Acta Cryst.* D**60**, 2126–2132.
Evans, P. (2006). *Acta Cryst.* D**62**, 72–82.
Fernández-Escamilla, A. M., Cheung, M. S., Vega, M. C., Wilmanns, M., Onuchic, J. N. & Serrano, L. (2004). *Proc. Natl Acad. Sci. USA*, **101**, 2834–2939.
Gill, S. C. & von Hippel, P. H. (1989). *Anal. Biochem.* **182**, 319–326.
Kabsch, W. (1976). *Acta Cryst.* A**32**, 922–923.
Krissinel, E. & Henrick, K. (2005). *CompLife 2005*, edited by M. R. Berthold, R. Glen, K. Diederichs, O. Kohlbacher & I. Fischer, pp. 163–174. Berlin/Heidelberg: Springer-Verlag.
Krissinel, E. & Henrick, K. (2007). *J. Mol. Biol.* **372**, 774–797.
Leslie, A. G. W. (2006). *Acta Cryst.* D**62**, 48–57.
Martinez, J. C., Pisabarro, M. T. & Serrano, L. (1998). *Nature Struct. Biol.* **5**, 721–729.
Martínez, J. C. & Serrano, L. (1999). *Nature Struct. Biol.* **6**, 1010–1016.
Morel, B., Casares, S. & Conejero-Lara, F. (2006). *J. Mol. Biol.* **356**, 453–468.
Musacchio, A., Noble, M., Pauptit, R., Wierenga, R. & Saraste, M. (1992). *Nature (London)*, **359**, 851–855.
Powell, H., Leslie, A. & Battye, G. (2007). *CCP4 Newsl.* **46**, contribution 1.
Vega, M. C., Martínez, J. C. & Serrano, L. (2000). *Protein Sci.* **9**, 2322–2328.
Ventura, S., Vega, M. C., Lacroix, E., Angrand, I., Spagnolo, L. & Serrano, L. (2002). *Nature Struct. Biol.* **9**, 485–493.
Viguera, A. R., Martínez, J. C., Filimonov, V. V., Mateo, P. L. & Serrano, L. (1994). *Biochemistry*, **33**, 2142–2150.
Zwart, P. H., Afonine, P. V., Grosse-Kunstleve, R. W., Hung, L.-W., Ioerger, T. R., McCoy, A. J., McKee, E., Moriarty, N. W., Read, R. J., Sacchettini, J. C., Sauter, N. K., Storoni, L. C., Terwilliger, T. C. & Adams, P. D. (2008). *Methods Mol. Biol.* **426**, 419–435.